

Phase Transformations in the Al–Mg Alloys Driven by High-Pressure Torsion

Olga Kogtenkova, Boris Borisovich Straumal,* Andrey Mazilkin, Tomasz Czeppe, and Pawel Zieba

As-cast aluminum–magnesium alloys with 3, 5, and 10 wt% Mg are subjected to high-pressure torsion (HPT) at room temperature: 5 GPa, five turns with rotation speed of 1 rpm. HPT leads to the strong grain refinement for both (Al) solid solution and intermetallic β -phase. Transmission electron microscopy (TEM), differential scanning calorimetry (DSC), and X-ray diffraction (XRD) are used to characterize the phase transitions under heating of the HPT-treated alloys. The decomposition of the solid solution in the ultrafine-grained Al–10 wt% Mg alloy obtained by HPT does not follow the equilibrium diagram. The results of DSC, XRD, and TEM show that the Mg-rich intermetallic phases appear during heating in the following sequence: GP zones $\rightarrow \beta \rightarrow \epsilon \rightarrow \beta \rightarrow \gamma \rightarrow \beta$. The (Al)/(Al) grain boundaries (GBs) in the fine-grained Al–10 wt% Mg alloy after HPT and annealing up to 400 °C (i.e., in the solid solution area, far from solvus and solidus lines) contain the Mg-rich areas. This can be the result of possible GB phase transitions with the formation of Mg-rich GB phases. The GBs in the binary Al–Mg can contain the thin layers of a GB phase far away from the solvus line.

deformation of Al–Mg-based alloys significantly affects the microstructure stability during following isothermal aging. It is because of the large density of dislocations. Dislocations serve as short-circuit diffusion paths for solutes^[17–19] and favorable nucleation sites for precipitates.^[16] It leads to the extensive heterogeneous precipitation along dislocations^[20,21] and modifies the precipitation sequence.^[8,9,11,15,22–31] Exactly speaking, the additional defects shift the precipitation sequence toward the formation of stable phases instead of metastable ones. In case of severe plastic deformation (SPD), not only the dislocations but also numerous grain boundaries (GBs) appear in a material.^[6,14] Therefore, the prior SPD can promote the formation of phases in new GBs and, therefore, accelerates the precipitation kinetics.^[6,14]

The industrial Al–Mg-based alloys usually have a low concentration of magnesium.^[2,5,8,11,18] Therefore, the study of Al–Mg model alloys with a low magnesium content is of great interest for researchers and, ultimately, for manufacturers.^[4,8,11,12,18,20] According to the magnesium content, all industrial aluminum–magnesium alloys are in the single-phase region of the (Al) solid solution (called also α -phase) of the Al–Mg phase diagram.^[2,4,5,12] Within the single-phase region of the (Al) phase, the parameter of the face centered cubic (fcc) lattice of (Al) matrix continuously increases with increasing magnesium content. The hardening of the alloys of this system is explained by an increase in the distortion of the crystal lattice with an increase in a portion of Mg atoms in the (Al) fcc lattice positions.^[2,4,5,12,19,20] Coarse-grained (as-cast) Al–Mg alloys with a small concentration of the second component in addition to the (Al) solid solution may contain the intermetallic phase(s) with a variable composition such as stable Al_3Mg_2 (or β -phase), R (or ϵ -phase), $\text{Al}_{12}\text{Mg}_{17}$ (or γ -phase), and metastable phases.^[1,4,5,8,11,16,19,22,25,35] To improve the mechanical properties of magnesium alloys, the ultrafine-grained and nanocrystalline alloys were developed applying the SPD.^[6,8,14,15,24] Such alloys have a large number of GBs along which interlayers of metastable phases can be formed during heat treatment.^[6,11,13,15]

Recently, the authors studied the samples of the Al–10 wt% Mg alloy in the single-phase region of Al–Mg phase diagram after SPD by high-pressure torsion (HPT).^[39] In this work, it was shown that such compounds as metastable phases appear after HPT in the single-phase region of the (Al) solid solution.

1. Introduction

The Al–Mg binary alloys^[1,2] are the base for the various ternary (mainly Al–Mg–Si)^[3–17] and multicomponent^[18–38] Al-based industrial alloys. Their unique mechanical properties are controlled by the formation of Guinier–Preston (GP) zones, metastable and stable intermetallic phases during thermal^[3,9,10,12,13,17–19,30,35] and mechanical^[6,7,9,11,15,31,35] pretreatment, and natural and artificial ageing.^[5,9,10,12,13,17,20,35] The alloying with additional components modifies the precipitation sequence and, consequently, the resulted mechanical properties.^[18–38] The plastic

O. Kogtenkova, B. B. Straumal, A. Mazilkin
Institute of Solid State Physics
Russian Academy of Sciences
Chernogolovka 142432, Russia
E-mail: straumal@mf.mpg.de, straumal@issp.ac.ru

O. Kogtenkova, B. B. Straumal
Department of Materials Science
Scientific Center of Russian Academy of Sciences
Chernogolovka 142432, Russia

T. Czeppe, P. Zieba
Institute of Metallurgy and Materials Science
Polish Academy of Sciences
Krakow 30-059, Poland

 The ORCID identification number(s) for the author(s) of this article can be found under <https://doi.org/10.1002/pssb.202100210>.

DOI: 10.1002/pssb.202100210

On the contrary, other authors^[40–43] found the metastable phases in the single-phase region of Al–Mg alloys.

Interpretation of metastable phases formed in the GBs causes some difficulty for researchers because there are disagreements in the construction of the equilibrium phase diagram of the Al–Mg system. There are several variants of the Al–Mg phase diagram with different number of phases and different representations of their chemical formulae.^[43–46] For example, according to Mikheeva,^[45] in Al–Mg alloys three more phases (β , β' , and γ) are formed apart from solid solutions which are separated by areas of heterogeneity. According to Mondolfo,^[44] the phase diagram of the Al–Mg system contains such compounds as $\beta(\text{Al}_8\text{Mg}_5)$, $\varepsilon(\text{Al}_{30}\text{Mg}_{23})$, $\text{Al}_{12}\text{Mg}_{17}$, $\text{Al}_8\text{Mg}_5 + \varepsilon$, and $\text{Al}_{12}\text{Mg}_{17} + \varepsilon$. In previous studies,^[47,48] the phases β , ε , and γ are given; in the study by Massalski,^[43] the phases Al_3Mg_2 (or β -phase), $\text{Al}_{12}\text{Mg}_{17}$ (or γ -phase), and R (or $\beta + \gamma$ -phases) are present.

To understand which processes precede the formation of metastable phases in the single-phase region of the α -solid solution and which phases stand out on the GB, we conducted studies in the two-phase region of phase diagram. For this purpose, we investigated the Al–Mg alloys with a low magnesium content of 3, 5, and 10 wt% after HPT treatment using the differential scanning calorimetry (DSC) in the temperature range from 25 to 400 °C. The goal of this work was to check whether (Al)/(Al)

GBs can contain the layers of a second phase “deep” in the (Al) region, i.e., far away from the solvus line of the phase diagram.

2. Results and Discussion

Figure 1 shows the micrographs of the Al–10 wt% Mg alloy in the as-cast state (Figure 1a), after HPT treatment (Figure 1b) and after heating in the DSC of the deformed sample (after HPT treatment) from 25 to 400 °C (Figure 1c). The scanning transmission electron microscopy (STEM) micrograph of the initial state of the as-cast Al–10 wt% Mg alloy (Figure 1a) shows that it contains a solid solution (Al) appearing light-gray and the β -phase (Al_3Mg_2) appearing dark. Inset shows the diffraction pattern of coarse-grained (Al) matrix. The β -phase has a shape of a crystalline colony with an average size of 2–3 μm . The average grain size of (Al) is 500 μm ; the dislocation density in (Al) is about 10^3 m^{-2} .^[49,50]

Figure 1b shows the transmission electron microscopy (TEM) micrograph of Al–10 wt% Mg alloy after HPT treatment (5 turns, 1 rpm). The average grain size of α -phase (Al) is 150 nm. The alloy structure is characterized by a high density of dislocations ($>10^3 \text{ m}^{-2}$) which indicates a high degree of internal strains. In accordance with the data of electron diffraction (see inset), the

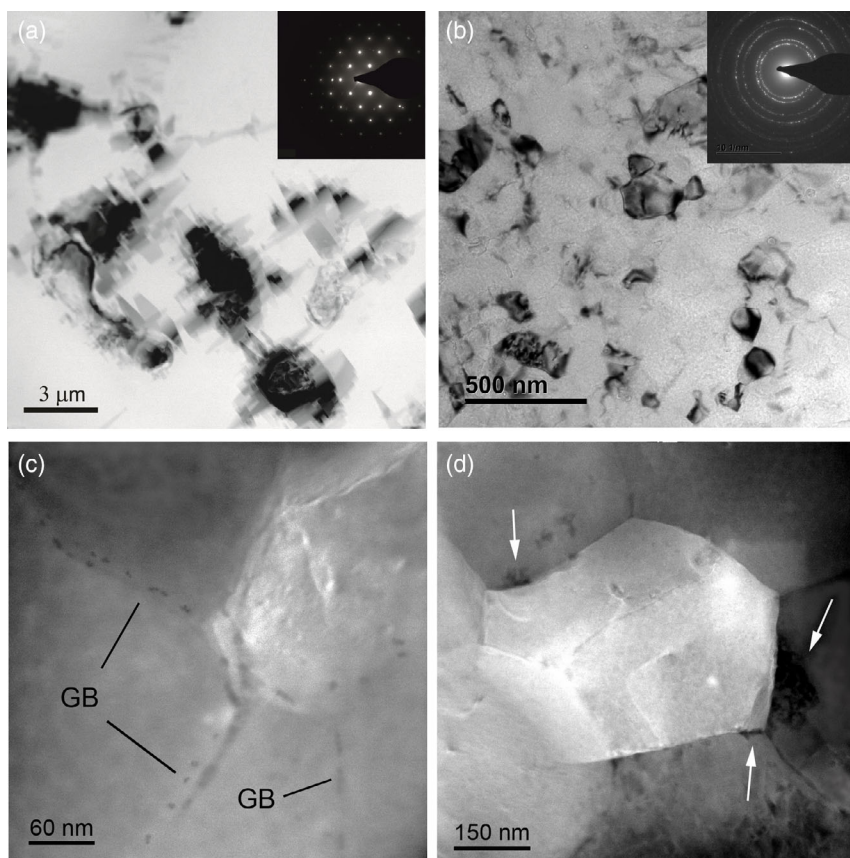


Figure 1. Microstructures of Al–10 wt% Mg alloy. a) STEM micrograph of as-cast alloy. Solid solution (Al) appears light-gray, the β -phase (Al_3Mg_2) appears dark. Inset shows the diffraction pattern of (Al) matrix. b) TEM micrograph of the same alloy after HPT. Inset shows the respective diffraction pattern. c,d) TEM micrograph of different areas in the same alloy after HPT and heating in DSC calorimeter up to $T = 400$ °C.

structure of the alloy after HPT contains the α -phase (Al) and intermetallic phase β with particle size is about 10 nm. These β nanoparticles are uniformly distributed throughout the volume of the material. Thus, the HPT leads to the strong grain refinement both of α - and β -phases.^[49,50]

Figure 1c shows the TEM micrograph of Al–10 wt% Mg alloy after HPT heated in DSC calorimeter up to 400 °C. According to the phase diagram, the temperature of 400 °C corresponds to the single-phase region of the solid solution (Al) far from the bulk solvus and solidus lines. Nevertheless, it can be seen that the (Al)/(Al) GBs contain separate particles of the β -phase. Figure 1d shows the TEM micrograph of another area of the same sample, as shown in Figure 1c. Small dark areas (shown by white arrows) are visible near the GBs. These areas are enriched in Mg (up to 28 wt% Mg), whereas the average magnesium content in the volume is 9 wt% Mg. The (Al) grains grew during heating up to 1 μ m (from 150 nm after HPT). It may indicate the abnormally rapid grain growth as a result of the formation of interlayers in the GBs. Similar abnormal grain growth was observed in industrial aluminum alloys in the work.^[51] The observed Mg-rich areas can be the result of possible GB phase transitions with the formation of Mg-rich GB phases. For example, the GB phases enriched by the alloying element(s) were observed in the Cu–Bi,^[52–54] Fe–Si–Zn,^[55,56] or Al–Zn^[57,58] alloys.

Figure 2 shows the temperature dependences of the heat flow (DSC curves) for Al–10 wt% Mg alloys before and after HPT treatment; Al–5 wt% Mg and Al–3 wt% Mg after HPT. We used the standard procedure for the quantification of the DSC curves^[59] (these procedures are also included in the quantification of the software of modern DSC equipment). According to this approach, the position of the deep minimum (peak) corresponds to the melting temperature, i.e., the liquidus temperature in the phase diagram. The position of the deep minimum (peak) is slightly influenced by the heating rate. Therefore, we used the same heating rate in all experiments. The onset temperature of the peak corresponds to the point of intersection of the tangent drawn through the inflexion point of the curve with the extrapolated baseline. The baseline is a virtual line drawn through the interval in which the phase transition takes place.

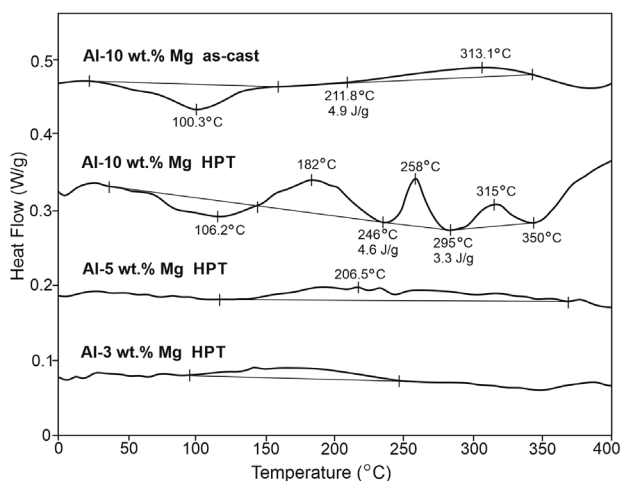


Figure 2. DSC curves of Al–10 wt% Mg as-cast and after HPT; Al–5 wt% Mg after HPT; Al–3 wt% Mg after HPT.

The great interest is the DSC curve for the Al–10 wt% Mg alloy after HPT treatment, which has a complex shape. It has one endothermic peak at $T = 106.2$ °C and three exothermic peaks at temperatures of 182, 258, and 315 °C. In alloys with a concentration of 3 and 5 wt% Mg (after HPT) and as-cast Al–10 wt% Mg alloy (before HPT), the shape of the DSC curves is different. Differently to our results, the Al–10 wt% Mg alloy after mechanical alloying (by ball milling) does not contain any β -phase.^[40] It appears only after heating in the calorimeter. Similar to our results, the DSC curves of mechanically alloyed samples contain several peaks.^[40] There are also works^[14,60–62] where the DSC curves for heating of Al–Mg alloys doped with third and more components also contain first one endothermic peak and then three exothermic peaks, such as our DSC curves for the Al–10 wt% Mg alloy after HPT (Figure 2, second curve from the top). These alloys were treated with other SPD methods such as ECAP (6013 Al–Mg–Si–Cu alloy),^[14] stretching (Al–Mg–Cu alloys),^[61] or cryomilling (Al–Mg–Sc alloy).^[62] Different sequence of processes hides under this superficial similarity of DSC curves. Thus, the formation of alloyed zones and S-phase proceeds by heating of stretched Al–Mg–Cu alloys^[61] or recovery, recrystallization, and precipitation of Al_3Sc phase takes place in Al–Mg–Sc alloys.^[62]

In order to understand, what is happening in our case in the Al–10 wt% Mg alloy after HPT, we heated the samples in the DSC to temperatures of 182, 258, 295, 315, and 350 °C, corresponding to peaks on the DSC curve. After heating the samples were tempered in water and examined using X-ray diffraction (XRD). According to DSC data, the first endothermic peak at the temperature of about 100 °C (as in the Al–10 wt% Mg alloys to HPT and Al–5 wt% Mg after HPT) corresponds to the decay of the GP zones and the start of formation of the β -phase. At $T = 182$ °C at the first exothermic peak (Figure 2), according to the data of X-ray structural analysis (see Figure 3), the β -phase is formed.

At the second exothermic peak at $T = 258$ °C, according to X-ray structural analysis (see Figure 3), the β -phase and ϵ -phase ($\text{Al}_{30}\text{Mg}_{23}$) are present in the structure. The XRD peak at an angle of $2\theta = 35.87^\circ$ is an overlap of the peaks of the ϵ -phase ($2\theta = 35.876^\circ$), the β -phase ($2\theta = 35.950^\circ$), and the γ -phase ($2\theta = 36.113^\circ$), so it is difficult to interpret this phase unambiguously. According to ref. [48], the ϵ -phase can exist in Al–Mg alloys at 250 °C. Therefore, we conclude that this peak corresponds to partial dissolution of the β -phase and formation of ϵ -phase, but do not exclude the possibility of the presence of the γ -phase in a small amount.

Some weak peaks are also present in Figure 3, for example, at 50.5° (25 °C), 42° (295 and 315 °C), 66° (258, 295, and 315 °C). They cannot be attributed to any of β -, γ -, or ϵ -phases. Therefore, we cannot exclude the presence of very small amounts of other (metastable) phases in the samples.

At $T = 295$ °C, corresponding to the endothermic peak (Figure 2), the β -phase is mainly present in the alloy and the ϵ -phase is dissolved. At $T = 315$ °C (exothermic maximum in Figure 2), the formation of the γ -phase occurs, but the β -phase is also present. At $T = 350$ °C, the γ -phase decomposes and the amount of the β -phase increases. Thus, the β -phase is formed as a result of the melting of the Al–10 wt% Mg alloy in the form of colonies; after HPT it is crushed, forming separate small precipitations. During heating of the deformed alloy up to 400 °C

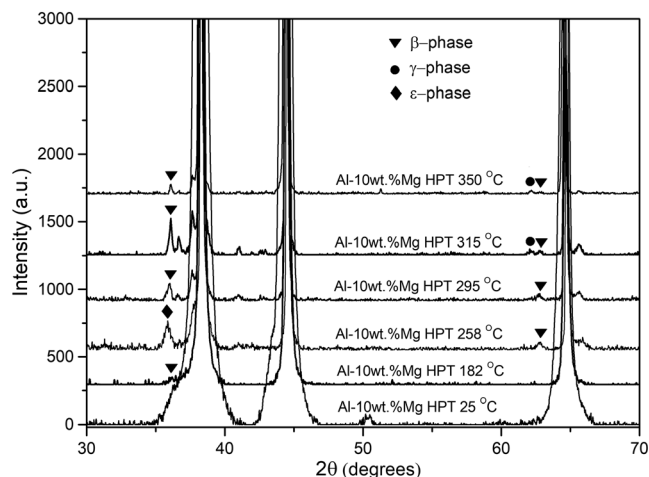


Figure 3. XRD patterns of the Al–10 wt% Mg alloy at different temperatures: 25, 182, 258, 295, 315, and 350 °C.

magnesium-based solid solution decomposes, the amount of β -phase changes (but it does not disappear) as a result of the formation and decomposition of new intermetallic ϵ - and γ -phases ($\beta \rightarrow \epsilon \rightarrow \beta \rightarrow \gamma \rightarrow \beta$).

The presence of β -phase in (Al)/(Al) GBs after heating up to 400 °C (Figure 1c,d) far away from the solvus line can be the indication of thin layers of a grain boundary phase rather “deep” in the one-phase area of a phase diagram in the binary Al–Mg alloy. For example, the GB phases enriched by the alloying element(s) were observed close to the solidus or solvus in the Cu–Bi,^[52–54] Fe–Si–Zn,^[55,56] or Al–Zn^[57,58] alloys.

3. Conclusions

The decomposition of the solid solution in the ultrafine-grained Al–10 wt% Mg alloy obtained by HPT does not follow the equilibrium diagram. The results of DSC, XRD, and TEM show that the Mg-rich phases appear during heating in following sequence: GP zones $\rightarrow \beta \rightarrow \epsilon \rightarrow \beta \rightarrow \gamma \rightarrow \beta$. The (Al)/(Al) GBs in the fine-grained Al–10 wt% Mg alloy after HPT and annealing up to 400 °C contain the Mg-rich areas. The temperature of 400 °C is in the solid solution area, i.e., far from solvus and solidus lines. Therefore, the observed Mg-rich areas can be the result of possible GB phase transitions with the formation of Mg-rich GB phases. Thus, the results of this work demonstrate that the GBs in the binary Al-based alloy can contain the thin layers of a GB phase rather “deep” in the one-phase area of a phase diagram. These results shed light on specific and poorly understood mechanisms of microstructure formation in the ultrafine-grained Al-based alloys. The presence of the GB phases has a potential for the future use for tailoring the properties of Al alloys for both structural needs and electrical engineering.

4. Experimental Section

The aluminum–magnesium alloys containing 3, 5, and 10 wt% Mg were prepared in the form of cylindrical ingots with a diameter of 10 mm using vacuum induction melting from highly pure components (5N5 Al and 4N5

Mg). For further research, the discs with a thickness of 3.5 and 0.7 mm were cut off from the ingots using electric-spark cutting. The discs in 0.7 mm thickness after chemical etching were subjected to severe plastic deformation by HPT in a Bridgman anvil-type unit (manufactured by W. Klement GmbH, Lang, Austria) at room temperature under a pressure of 5 GPa (5 turns, 1 rpm). For the structural studies and calorimetric measurements in the alloys before HPT treatment (3.5 mm thickness disks) and after HPT treatment (0.7 mm thickness disks), samples with a diameter of 3 mm with the center in the middle of the disk radius were cut in the disc. The samples were heated in a DSC TA Instruments 910 or 1600 from room temperature to 400 °C at the rate of 10 K min^{−1}. After heating, the samples were cooled in a calorimeter to room temperature at the rate of about 10 K s^{−1}. TEM was conducted on Philips CM 20, TECNAI G2 F20 microscopes, and with TECNAI G2 FEG super TWIN (200 kV) transmission electron microscope equipped with energy-dispersive X-ray spectroscopy (EDS) system manufactured by EDAX with accelerating voltages of 200 kV. XRD analysis was performed on Siemens D-500 with Cu K α radiation ($\lambda = 0.15406$ nm). The samples for XRD and TEM were heated up to a certain temperature of 182, 258, 295, 315, and 350 °C (see Figure 3) in calorimeter to obtain the same states as during continuous DSC with the same heating and cooling rate of 10 K min^{−1}. The mean size of the (Al) grains (α -phase) and that of crystalline colonies of β -phase (Al₃Mg₂) were estimated using STEM micrographs as an average value for about 100–200 grains or colonies.

Acknowledgements

The research was conducted within the state task of ISSP RAS and in the frame of bilateral scientific cooperation between ISSP RAS and IMMS PAS. The TEM and DSC measurements were performed within the Accredited Testing Laboratories possessing the certificate no. AB 120 issued by the Polish Centre of Accreditation according to European standard PN-ISO/IEC 321 17025:2005 as well as the EA-2/15.

Conflict of Interest

The authors declare no conflict of interest.

Data Availability Statement

Research data are not shared.

Keywords

Al–Mg alloys, high-pressure torsion, phase transformations

Received: May 15, 2021

Revised: August 3, 2021

Published online:

- [1] M. Liu, B. Klobes, J. Banhart, *J. Mater. Sci.* **2016**, *51*, 7754.
- [2] M. Fatmi, F. Sahnoune, H. Belhouchet, T. Chihi, M. A. Ghebouli, B. Ghebouli, B. Barka, T. Rechidi, *Chin. J. Phys.* **2016**, *2*, 216.
- [3] X. Duan, Z. Mi, H. Jiang, Y. Wu, W. Jiayi, *Mater. Res. Express* **2019**, *7*, 076576.
- [4] M. Afshar, F. Mao, H. Jiang, V. Mohles, M. Schick, K. Hack, S. Korte-Kerzel, L. A. Barrales-Mora, *Comput. Mater. Sci.* **2019**, *158*, 235.
- [5] M. Madanat, M. Liu, J. Banhart, *Acta Mater.* **2018**, *159*, 163.
- [6] T. Khelifa, M. A. Rekik, M. Khitouni, J. M. Cabrera-Marrero, *Int. J. Adv. Manuf. Technol.* **2017**, *92*, 1731.

- [7] Y. Wang, K. Zhang, W. Wu, W. Wang, J. Wang, *Mater. Sci. Eng. A* **2017**, 703, 559.
- [8] A. Chbihi, S. Vincent, J. Ribis, C. Toffolon-Masclat, J. Garnier, *J. Mater. Sci.* **2017**, 52, 6063.
- [9] Z. Jia, L. Ding, Y. Weng, Z. Wen, Q. Liu, *Trans. Nonferrous Met. Soc. China* **2016**, 26, 924.
- [10] H. Nemour, D. M. Ibrahim, A. Triki, *J. Therm. Anal. Calorim.* **2016**, 123, 19.
- [11] T. Ogura, K. Horikawa, Y. Kitani, M. Miara, S. N. Kim, E. Kobayashi, T. Sato, H. Kobayashi, *Mater. Trans.* **2016**, 57, 1282.
- [12] B. Milkereit, M. J. Starink, *Mater. Des.* **2015**, 76, 117.
- [13] M. Mihara, E. Kobayashi, T. Sato, *Mater. Trans.* **2015**, 56, 500.
- [14] M. Liu, T. Jiang, J. Wang, Q. Liu, Z. Wu, Y. Yu, P. C. Skaret, H. J. Roven, *Trans. Nonferrous Met. Soc. China* **2014**, 24, 3858.
- [15] P. N. Rao, D. Singh, R. Jayaganthan, *J. Mater. Sci. Technol.* **2014**, 10, 998.
- [16] S. N. Kim, J. H. Kim, E. Kobayashi, T. Sato, *Mater. Trans.* **2014**, 11, 1647.
- [17] Z. Zhang, H. Xu, S. Wu, Y. Liu, *Acta Metall. Sin.* **2013**, 26, 340.
- [18] H. Li, Z. Yan, L. Cao, *Mater. Sci. Eng. A* **2018**, 728, 88.
- [19] S. Jin, T. Ngai, L. Li, Y. Lai, Z. Chen, A. Wang, *J. Alloys Compd.* **2018**, 742, 852.
- [20] G. W. Zheng, H. Li, C. Lei, J. Fu, T. J. Bian, J. C. Yang, *Mater. Sci. Eng. A* **2018**, 718, 157.
- [21] Y. Birol, *Thermochim. Acta* **2017**, 650, 39.
- [22] Y. Weng, Z. Jia, L. Ding, Y. Pan, Y. Liu, Q. Liu, *J. Alloys Compd.* **2017**, 695, 2444.
- [23] M. X. Guo, X. K. Zhang, J. S. Zhang, L. Z. Zhuang, *J. Mater. Sci.* **2017**, 52, 1390.
- [24] L. Ding, Z. Jia, Y. Liu, Y. Weng, Q. Liu, *J. Alloys Compd.* **2016**, 688, 362.
- [25] M. X. Guo, Y. Zhang, X. K. Zhang, J. S. Zhang, L. Z. Zhuang, *Mater. Sci. Eng. A* **2016**, 669, 20.
- [26] J. T. Liu, Y. A. Zhang, X. W. Li, Z. H. Li, B. Q. Xiong, J. S. Zhang, *Rare Met.* **2016**, 35, 380.
- [27] J. H. Kim, E. Kobayashi, T. Sato, *Mater. Trans.* **2015**, 11, 1771.
- [28] M. X. Guo, G. Sha, L. Y. Cao, W. Q. Liu, J. S. Zhang, L. Z. Zhuang, *Mater. Chem. Phys.* **2015**, 162, 15.
- [29] M. Liu, Z. Wu, R. Yang, J. Wei, Y. Yu, P. C. Skaret, H. J. Roven, *Prog. Nat. Sci. Mater. Int.* **2015**, 25, 153.
- [30] L. Ding, Z. Jia, Z. Zhang, R. E. Sanders, Q. Liu, G. Yang, *Mater. Sci. Eng. A* **2015**, 627, 119.
- [31] U. D. Shamas, J. Kamran, B. A. Hasan, N. H. Tariq, M. Mehmood, M. Z. Shamas, *Mater. Des.* **2014**, 64, 366.
- [32] P. Lang, E. Povoden-Karadeniz, A. Falahati, E. Kozeschnik, *J. Alloys Compd.* **2014**, 612, 443.
- [33] C. Liu, X. Zhang, J. Tang, X. Liu, L. Chen, *Trans. Nonferrous Met. Soc. China* **2014**, 24, 2289.
- [34] J. Tian, K. D. Woo, K. J. Lee, Y. Chen, *Korean J. Met. Mater.* **2014**, 52, 101.
- [35] M. Mihara, E. Kobayashi, T. Sato, *Mater. Trans.* **2013**, 54, 1898.
- [36] S. Wang, S. S. Chen, K. Matsuda, T. Kawabata, J. Nakamura, S. Ikeno, K. Kawakita, H. Takagi, T. Yamashita, *Mater. Trans.* **2012**, 53, 1521.
- [37] J. H. Kim, H. Tezuka, E. Kobayashi, T. Sato, *Korean J. Mater. Res.* **2012**, 22, 329.
- [38] H. Zhang, Z. Zheng, Y. Lin, *J. Mater. Sci.* **2012**, 47, 4101.
- [39] O. Kogtenkova, B. Straumal, *Metals* **2019**, 9, 10.
- [40] M. Schoenitz, E. L. Dreizin, *J. Mater. Res.* **2003**, 18, 1827.
- [41] M. Boucheur, D. Hamana, T. Laoui, *Philos. Mag. A* **2019**, 73, 1733.
- [42] I. S. Golovin, A. V. Mikhaylovskaya, H. R. Sinning, *J. Alloys Compd.* **2013**, 577, 622.
- [43] T. B. Massalski, *Binary Alloy Phase Diagrams*, 2nd ed., ASM International, Materials Park, OH **1990**.
- [44] L. F. Mondolfo, *Aluminium Alloys: Structure and Properties*, Butterworths, London **1976**.
- [45] V. I. Mikheeva, *Alloys of Magnesium with Aluminum and Zinc*, Institute of General and Inorganic Chemistry named after N.S. Kurnakova, Moscow, **1946**.
- [46] E. Shurmann, H. J. Voss, *Giessereiforschung* **1981**, 33, 43.
- [47] B. Predel, K. Hulse, *Z. Metallkunde* **1978**, 69, 690.
- [48] Y. Zhong, M. Yang, Z. K. Liu, *Calphad* **2005**, 29, 303.
- [49] B. B. Straumal, B. Baretzky, A. A. Mazilkin, F. Phillipp, O. A. Kogtenkova, M. N. Volkov, R. Z. Valiev, *Acta Mater.* **2004**, 52, 4469.
- [50] A. A. Mazilkin, B. B. Straumal, E. Rabkin, B. Baretzky, S. Enders, S. G. Protasova, O. A. Kogtenkova, R. Z. Valiev, *Acta Mater.* **2006**, 54, 3933.
- [51] V. N. Perevezentsev, M. Y. Shcherban, M. Y. Murashkin, R. Z. Valiev, *Tech. Phys. Lett.* **2007**, 33, 648.
- [52] L. S. Chang, B. B. Straumal, E. Rabkin, W. Gust, F. Sommer, *J. Phase Equilib.* **1997**, 18, 128.
- [53] L. S. Chang, E. Rabkin, B. B. Straumal, S. Hoffmann, B. Baretzky, W. Gust, *Defects Diffus. Forum* **1998**, 156, 135.
- [54] L. S. Chang, E. Rabkin, B. Straumal, P. Lejcek, S. Hofmann, W. Gust, *Scr. Mater.* **1997**, 37, 729.
- [55] O. I. Noskovich, E. I. Rabkin, V. N. Semenov, B. B. Straumal, L. S. Shvindlerman, *Acta Metall. Mater.* **1991**, 39, 3091.
- [56] B. B. Straumal, O. I. Noskovich, V. N. Semenov, L. S. Shvindlerman, W. Gust, B. Predel, *Acta Metall. Mater.* **1992**, 40, 795.
- [57] B. B. Straumal, O. A. Kogtenkova, A. B. Straumal, B. Baretzky, *Lett. Mater.* **2018**, 8, 364.
- [58] B. B. Straumal, A. A. Mazilkin, X. Sauvage, R. Z. Valiev, A. B. Straumal, A. M. Gusak, *Russ. J. Non-ferrous Met.* **2015**, 56, 44.
- [59] J. A. Dean, *The Analytical Chemistry Handbook*, McGraw Hill, New York **1995**.
- [60] N. Gao, M. J. Starink, T. G. Langdon, *Mater. Sci. Technol.* **2009**, 25, 687.
- [61] N. Gao, L. Davin, S. Wang, A. Cerezo, M. J. Starink, *Mater. Sci. Forum* **2002**, 396–402, 923.
- [62] F. Zhou, Z. Lee, E. J. Lavernia, S. R. Nutt, *Metall. Mater. Trans. A* **2005**, 36A, 1587.